united nations
educational, scientific
and cultural
organization

international atomic
energy agency

the
abdus salam
international centre for theoretical physics

40th anniversary 1964 2004

H4.SMR/1586-8

"7th Workshop on Three-Dimensional Modelling
of Seismic Waves Generation and their Propagation"

25 October - 5 November 2004

Surface Wave Inversion for Source Parameters. Surface Wave Focusing

B.G. Bukchin
International Institute of Earthquake Prediction
Theory and Mathematical Geophysics
Moscow, Russia

Surface wave inversion for source parameters. Surface wave focusing.

B.G. Bukchin
International Institute of Earthquake Prediction Theory and Mathematical Geophysics, Moscow, Russia

I. Formal description of seismic source

The description of seismic source we will consider is based on the formalism developed by Backus and Mulcahy, 1976.

Statement of the problem.

Motion equation

$$\rho \ddot{u}_i = \sigma_{ij,j} + f_i \qquad (1.1)$$

Hook's law for isotropic medium

$$\sigma_{ij} = \lambda \delta_{ij} \varepsilon_{kk} + 2\mu \varepsilon_{ij} \qquad (1.2)$$

Initial conditions

$$\dot{\mathbf{u}} \equiv \mathbf{u} \equiv 0, t < 0 \qquad (1.3)$$

Boundary conditions

$$\sigma_{ij} n_j |_{S_0} = 0 \qquad (1.4)$$

Here **u** – displacement vector; σ_{ij} – elements of symmetric 3x3 stress tensor; i,j=1,2,3 and the summation convention for repeated subscripts is used; $\sigma_{ij,j} = \sum_{j=1}^{3} \frac{\partial \sigma_{ij}}{\partial x_j}$; ε_{ij} – elements of symmetric 3x3 strain tensor and $\varepsilon_{ij} = 0.5(u_{i,j} + u_{j,i})$; ρ - density; f_i – components of external force; n_j – components of the normal to the free surface S_0.

Solution of the problem (1.1)-(1.4) can be given by formula

$$u_i(\mathbf{x},t) = \int_0^T d\tau \int_\Omega G_{ij}(\mathbf{x},\mathbf{y},t-\tau) f_j(\mathbf{y},\tau) dV_y \qquad (1.5)$$

or

$$u_i(\mathbf{x},t) = \int_0^T d\tau \int_\Omega H_{ij}(\mathbf{x},\mathbf{y},t-\tau) \dot{f}_j(\mathbf{y},\tau) dV_y \qquad (1.6)$$

Here G_{ij} is the Green's function,

$$H_{ij}(\mathbf{x},\mathbf{y},t) = \int_0^t G_{ij}(\mathbf{x},\mathbf{y},\tau) d\tau, \qquad (1.7)$$

$\mathbf{x} \in \Omega$ and $0 < t < T$ are the space region and time interval where $\dot{f}$ is not identically zero.

Sources of seismic disturbances

We will consider internal sources only (earthquakes). In this case any external forces are absent. We must then set $\mathbf{f} \equiv 0$ in equation (1.1), so that the only solution that satisfies the homogeneous initial (1.3) and boundary (1.4) conditions, as well as Hook's law (1.2) will be $\mathbf{u} \equiv 0$. Non-zero displacements cannot arise in the medium, unless at least one of the above conditions is not true.

Following Backus and Mulcahy, 1976, we assume seismic motion to be caused by a departure from ideal elasticity (from Hook's law) within some volume of the medium Ω at some time interval $0 < t < T$.

Let $\mathbf{u}(\mathbf{x},t)$ be the actual displacements, $\boldsymbol{\sigma}(\mathbf{x},t)$ - correspondent stresses, if Hook's law is valid, $\mathbf{s}(\mathbf{x},t)$ - actual stresses.

Let the difference

$$\boldsymbol{\Gamma}(\mathbf{x},t) = \boldsymbol{\sigma}(\mathbf{x},t) - \mathbf{s}(\mathbf{x},t), \qquad (1.8)$$

called the *stress glut tensor* or *moment tensor density*, is not identically zero for $0 < t < T$ and $\mathbf{x} \in \Omega$.

T we define as source duration, and Ω - source region. Within this region and time interval (and only there) the tensor $\dot{\mathbf{\Gamma}}(\mathbf{x},t)$ is not identically zero as well.

Replacing $\boldsymbol{\sigma}(\mathbf{x},t)$ by $\mathbf{s}(\mathbf{x},t)$ in equation (1.1), using definition (1.8) and the absence of external forces ($\mathbf{f} \equiv 0$) we can rewrite the motion equation (1.1) in form

$$\rho \ddot{u}_i = s_{ij,j}$$

or

$$\rho \ddot{u}_i = \sigma_{ij,j} + g_i \qquad (1.9)$$

where

$$g_i = -\Gamma_{ij,j} \ . \qquad (1.10)$$

Equation (1.10) defines the equivalent force **g**. Using formula (1.6) with f_i replaced by g_i , definition (1.10) and Gauss theorem we have for displacements

$$u_i(\mathbf{x},t) = \int_0^T d\tau \int_\Omega H_{ij,k}(\mathbf{x},\mathbf{y},t-\tau)\dot{\Gamma}_{jk}(\mathbf{y},\tau)dV_y \,, \qquad (1.11)$$

where H_{ij} is differentiated with respect to y_k .

If the inelastic motions are concentrated at a surface Σ, then

$$u_i(\mathbf{x},t) = \int_0^T d\tau \int_\Sigma H_{ij,k}(\mathbf{x},\mathbf{y},t-\tau)\dot{\Gamma}_{jk}(\mathbf{y},\tau)d\Sigma_y \,. \qquad (1.12)$$

Relation of stress glut (moment tensor density) with classic definition of moment tensor M :

$$\mathbf{M} = \int_0^T dt \int_\Omega \dot{\mathbf{\Gamma}}(\mathbf{y},t)dV_y \quad . \qquad (1.13)$$

Normalizing moment tensor we define seismic moment M_0 :

$\mathbf{M}=M_0\mathbf{m}$, where tensor **m** is normalized by condition $\mathrm{tr}(\mathbf{m}^{\mathrm{T}}\mathbf{m}) = \sum_{i,j=1}^{3} m_{ij}^2 = 2$, $\mathbf{m}^{\mathrm{T}}$ is transposed tensor **m**.

Stress glut moment for special types of seismic sources

1. Discontinuity of displacement $\Delta\mathbf{u}$ at a surface Σ in isotropic medium (stress is continuous):

$$\Gamma_{ij}(\mathbf{x},t) = \lambda \Delta u_k(\mathbf{x},t) n_k(\mathbf{x}) \delta_{ij} + \mu[n_i(\mathbf{x})\Delta u_j(\mathbf{x},t) + n_j(\mathbf{x})\Delta u_i(\mathbf{x},t)]. \qquad (1.14)$$

Here $\mathbf{n}(\mathbf{x})$ is the normal to the surface Σ, and seismic disturbances are given by formula (1.12).

2. In the case of tangential (shear) dislocation we have

$\Delta u_k n_k \equiv 0$ and formula (1.14) takes form

$$\Gamma_{ij}(\mathbf{x},t) = \mu[n_i(\mathbf{x})\Delta u_j(\mathbf{x},t) + n_j(\mathbf{x})\Delta u_i(\mathbf{x},t)]. \qquad (1.15)$$

3. Instant point tangential dislocation occurred in the point $\mathbf{x}=\mathbf{0}$ at time t=0:

$$\dot{\Gamma}_{ij}(\mathbf{x},t) = M_0 m_{ij} \delta(t)\delta(\mathbf{x}), \qquad (1.16)$$

where $m_{ij} = n_i a_j + n_j a_i$, $\mathbf{a} = \Delta\mathbf{u}/|\Delta\mathbf{u}|$ and $M_0 = \mu \, |\Delta\mathbf{u}|$.

Phenomena of matrix **m**

Tr**m** = 0. The eigenvalues of matrix **m** are: 1, -1 and 0. The eigenvector correspondent to 1 defines the direction of maximum extension, and the eigenvector correspondent to -1 defines the direction of maximum compression. Such a source is called double couple.

As it follows from formula (1.12) an instant point double couple excites a displacement field of the form

$$u_i(\mathbf{x},t) = M_0 H_{ik,l}(\mathbf{x},\mathbf{0},t) m_{kl} \,. \tag{1.17}$$

We have for Fourier transforms $\mathbf{H}(\mathbf{x},\mathbf{y},\omega)$ and $\mathbf{G}(\mathbf{x},\mathbf{y},\omega)$ from equation (1.7):

$$\mathbf{H}(\mathbf{x},\mathbf{y},\omega) = \frac{1}{\mathrm{i}\omega}\mathbf{G}(\mathbf{x},\mathbf{y},\omega)\,, \tag{1.18}$$

where i is the imaginary unit, and ω is angular frequency.
As result the spectrum of displacements is given by formula

$$u_i(\mathbf{x},\omega) = \frac{1}{\mathrm{i}\omega} M_0 m_{kl} G_{ik,l}(\mathbf{x},\mathbf{0},\omega)\,. \tag{1.19}$$

Relation between the displacement field and stress glut moments

We assume that following product can represent the time derivative of stress glut tensor:

$$\dot{\boldsymbol{\Gamma}}(\mathbf{x},t) = f(\mathbf{x},t)\mathbf{m}\,, \tag{1.20}$$

where $f(\mathbf{x},t)$ is non-negative function and **m** is a uniform normalized moment tensor.

The moment $f^{(l,n)}_{k_1\ldots k_l}(\mathbf{q},\tau)$ of spatial degree *l* and temporal degree *n* with respect to point **q** and instant of time τ is a tensor of order *l* and is given by formula

$$f^{(l,n)}_{k_1\ldots k_l}(\mathbf{q},\tau) = \int_V dV \int_0^\infty f(\mathbf{x},t)(x_{k_1}-q_{k_1})\cdots(x_{k_l}-q_{k_l})(t-\tau)^n dt\,, \tag{1.21}$$

$k_1,\ldots,k_l$=1,2,3.

Replacing $H_{ij}(\mathbf{x},\mathbf{y},t\text{-}\tau)$ in equation (1.11) by its Taylor series in powers of **y** and in powers of τ, we get:

$$u_i(\mathbf{x},t) = \sum_{l=0}^{\infty}\sum_{n=0}^{\infty}\frac{(-1)^n}{l!\,n!} m_{jk} f^{(l,n)}_{k_1\ldots k_l}(\mathbf{0},0)\frac{\partial^n}{\partial t^n}\frac{\partial}{\partial y_{k_1}}\cdots\frac{\partial}{\partial y_{k_l}}\frac{\partial}{\partial y_k} H_{ij}(\mathbf{x},\mathbf{y},t)\Big|_{\mathbf{y}=\mathbf{0}}\,. \tag{1.22}$$

Using formulae (1.18) and (1.22) we have following equation for the spectrum of displacements:

$$u_i(\mathbf{x},\omega) = \sum_{l=0}^{\infty}\sum_{n=0}^{\infty}\frac{(-1)^n}{l!\,n!} m_{jk} f^{(l,n)}_{k_1\ldots k_l}(\mathbf{0},0)(\mathrm{i}\omega)^{n-1}\frac{\partial}{\partial y_{k_1}}\cdots\frac{\partial}{\partial y_{k_l}}\frac{\partial}{\partial y_k} G_{ij}(\mathbf{x},\mathbf{y},\omega)\Big|_{\mathbf{y}=\mathbf{0}}\,. \tag{1.23}$$

Here we assume that the point **y**=**0** and the instant *t*=0 belong to the source region and the time of the source activity respectively.

When the spectra of displacements $u_i(\mathbf{x},\omega)$ and Green's function $G_{ij}(\mathbf{x},\mathbf{y},\omega)$ have been low pass filtered, the terms in equation (1.23) start to decrease with *l* and *n* increasing at least as rapidly as $(\omega T)^{l+n}$ (T is the source duration, and ωT<1), and one might then restrict to considering finite sums only.

We will take into account in the following sections only the first terms in formula (1.23) for $l + n \le 2$.

II. Source inversion in moment tensor approximation

The first term in (1.23) corresponding to *l*=0, *n*=0, describes the spectra of displacements $u_i(\mathbf{x},\omega)$ excited by an instant point source (compare with formula (1.19) taking into account that seismic moment is equal to zero moment of function $f(\mathbf{x},t)$: $M_0=f^{(0,0)}$). For a source with

nonzero size and duration this term approximates $u_i(\mathbf{x},\omega)$ with high accuracy for periods much longer then source duration. Performing the inversion of long period seismic waves we describe the earthquake by an instant point source. As it was mentioned in previous section, an instant point source can be given by moment tensor - a symmetric 3x3 matrix $\mathbf{M}$. Seismic moment M_0 is defined by equation $M_0 = \sqrt{1/2\,\mathrm{tr}(\mathbf{M}^{\mathrm{T}}\mathbf{M})}$, where $\mathbf{M}^{\mathrm{T}}$ is transposed moment tensor $\mathbf{M}$, and $\mathrm{tr}(\mathbf{M}^{\mathrm{T}}\mathbf{M}) = \sum_{i,j=1}^{3} M_{ij}^{\,2}$. Moment tensor of any event can be presented in the form $\mathbf{M} = M_0\mathbf{m}$, where matrix $\mathbf{m}$ is normalized by condition $\mathrm{tr}(\mathbf{m}^{\mathrm{T}}\mathbf{m}) = 2$.

We'll consider a double couple instant point source (a pure tangential dislocation) at a depth h. Such a source can be given by 5 parameters: double couple depth, its focal mechanism which is characterizing by three angles: strike, dip and slip or by two unit vectors (direction of principal tension **T** and direction of principal compression **P**) and seismic moment M_0. Four of these parameters we determine by a systematic exploration of the four dimensional parametric space, and the 5-th parameter M_0 - solving the problem of minimization of the misfit between observed and calculated surface wave amplitude spectra for every current combination of all other parameters.

Under assumptions mentioned above the relation between the spectrum of displacements $u_i(\mathbf{x},\omega)$ and moment tensor $\mathbf{M}$ can be expressed by formula (1.19) rewritten below in slightly different form:

$$u_i(\mathbf{x},\omega) = \frac{1}{\mathrm{i}\,\omega}[M_{jl}\frac{\partial}{\partial y_l}G_{ij}(\mathbf{x},\mathbf{y},\omega)] \qquad (2.1)$$

i,j = 1,2,3 and the summation convention for repeated subscripts is used. $G_{ij}(\mathbf{x},\mathbf{y},\omega)$ in equation (2.1) is the spectrum of Green function for the chosen model of medium and wave type (see Levshin, 1985; Bukchin, 1990), **y** - source location. We will discuss the inversion of surface wave spectra, so $G_{ij}(\mathbf{x},\mathbf{y},\omega)$ is the spectrum of surface wave Green function. We assume that the paths from the earthquake source to seismic stations are relatively simple and are well approximated by weak laterally inhomogeneous model (Woodhouse, 1974; Babich *et al.*, 1976). The surface wave Green function in this approximation is determined by the near source and near receiver velocity structure, by the mean phase velocity of wave, and by geometrical spreading. We assume that waves propagate from the source to station along great circles. Under these assumptions the amplitude spectrum $|u_i(\mathbf{x},\omega)|$ defined by formula (2.1) does not depend on the average phase velocity of the wave. In such a model the errors in source location do not affect the amplitude spectrum (Bukchin, 1990). The average phase velocities of surface waves are usually not well known. For this reason as a rule we use only amplitude spectra of surface waves for determining source parameters under consideration. We use observed surface wave phase spectra only for very long periods. Correcting the spectra for attenuation we use laterally homogeneous model for quality factor. At the end of this lecture we will consider the effects related to surface wave focusing caused by rays deviation from great circle, and to laterally inhomogeneity of attenuation model.

Surface wave amplitude spectra inversion

If all characteristics of the medium are known, the representation (2.1) gives us a system of equations for parameters defined above. Let us consider now a grid in the space of these 4 parameters. Let the models of the media be given. Using formula (2.1) we can calculate the amplitude spectra of surface waves at the points of observation for every possible combination of values of the varying parameters. Comparison of calculated and observed

amplitude spectra give us a residual $\varepsilon^{(i)}$ for every point of observation, every wave and every frequency ω. Let $u^{(i)}(\mathbf{x},\omega)$ be any observed value of the spectrum, i = 1,…,N; $\varepsilon^{(i)}_{\text{amp}}$ - corresponding residual of $|u^{(i)}(\mathbf{x},\omega)|$. We define the normalized amplitude residual by formula

$$\varepsilon_{\text{amp}}(h,\mathbf{T},\mathbf{P}) = \left[\left(\sum_{i=1}^{N} \varepsilon_{\text{amp}}^{(i)\,2}\right) \Big/ \left(\sum_{i=1}^{N} |u^{(i)}(\mathbf{x},\omega|^2\right)\right]^{1/2}. \qquad (2.2)$$

The optimal values of the parameters that minimize ε_{amp} we consider as estimates of these parameters. We search them by a systematic exploration of the four-dimensional parameter space. To characterize the degree of resolution of every of these source characteristics we calculate partial residual functions. Fixing the value of one of varying parameters we put in correspondence to it a minimal value of the residual ε_{amp} on the set of all possible values of the other parameters. In this way we define one residual function on scalar argument and two residual functions on vector argument corresponding to the scalar and two vector varying parameters: $\varepsilon_h(h)$, $\varepsilon_{\mathbf{T}}(\mathbf{T})$ and $\varepsilon_{\mathbf{P}}(\mathbf{P})$. The value of the parameter for which the corresponding function of the residual attains its minimum we define as estimate of this parameter. At the same time these functions characterize the degree of resolution of the corresponding parameters. From geometrical point of view these functions describe the lower boundaries of projections of the 4-D surface of functional ε on the coordinate planes. A sketch illustrating the definition of partial residual functions is given in figure 1.

Here one of 4 parameters is picked out as ‘parameter 1’, and one of coordinate axis corresponds to this parameter. Another coordinate axis we consider formally as 3-D space of the rest 3 parameters. Plane Σ is orthogonal to the axis ‘parameter 1’ and cross it in a point p_0. Curve L is the intersection of the plane Σ and the surface of functional ε. As one can see from the figure the point $\varepsilon_1(p_0)$ belong to the boundary of projection of the surface of functional ε, and at the same time it corresponds to a minimal value of the residual ε on the set of all possible values of the other 3 parameters while ‘parameter 1’ is equal to the value p_0. So, as it is accepted in engineering we characterize our surface by its 4 projections on coordinate planes.

It is well known that the focal mechanism cannot be uniquely determined from surface wave amplitude spectra. There are four different focal mechanisms radiating the same surface wave amplitude spectra. These four equivalent solutions represent two pairs of mechanisms symmetric with respect to the vertical axis, and within the pair differ from each other by the opposite direction of slip.

To get a unique solution for the focal mechanism we have to use in the inversion additional observations. For these purpose we use very long period phase spectra of surface waves or polarities of P wave first arrivals.

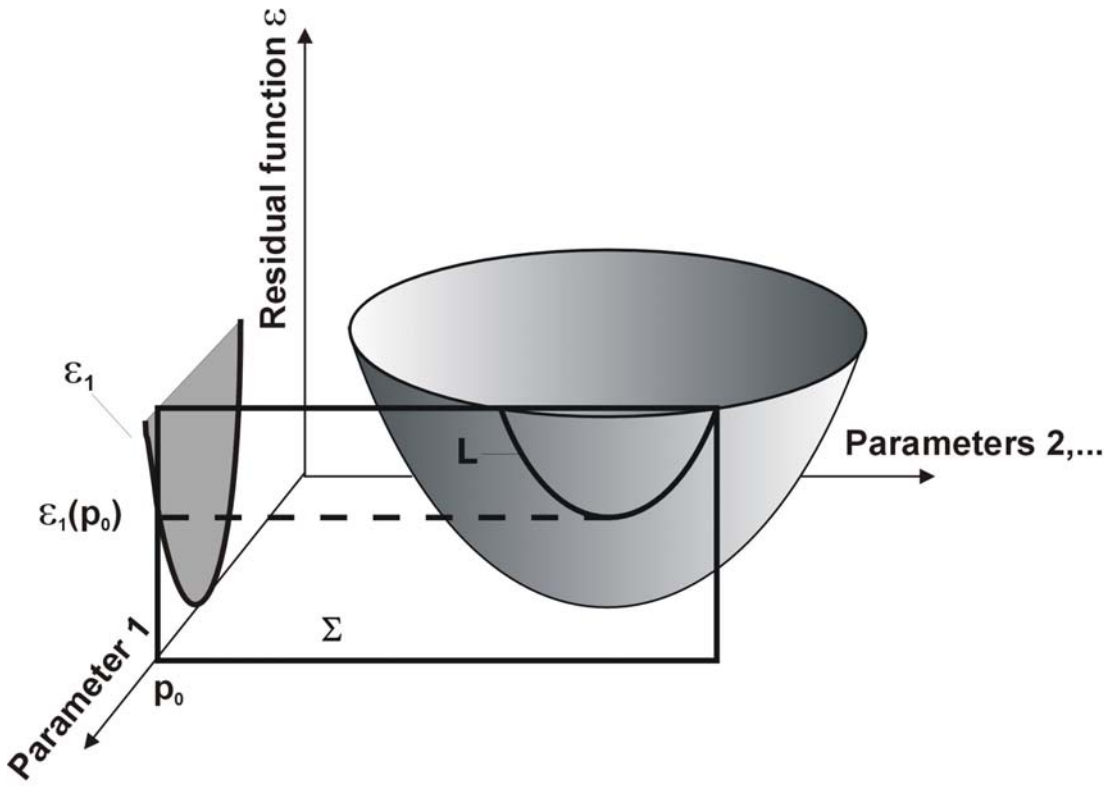

Figure 1. A sketch illustrating the definition of partial residual functions.

Joint inversion of surface wave amplitude and phase spectra

Using formula (2.1) we can calculate for chosen frequency range the phase spectra of surface waves at the points of observation for every possible combination of values of the varying parameters. Comparison of calculated and observed phase spectra give us a residual $\varepsilon_{\mathrm{ph}}^{(i)}$ for every point of observation, every wave and every frequency ω. We define the normalized phase residual by formula

$$\varepsilon_{\mathrm{ph}}(h, \varphi, \mathbf{T}, \mathbf{P}) = \frac{1}{\pi}\left[\left(\sum_{i=1}^{\mathrm{N}} \varepsilon_{\mathrm{ph}}^{(i)2}\right) / \mathrm{N}\right]^{1/2}. \qquad (2.3)$$

We determine the joint residual ε by formula

$$\varepsilon = 1 - (1 - \varepsilon_{\mathrm{ph}})(1 - \varepsilon_{\mathrm{amp}}). \qquad (2.4)$$

To characterize the resolution of source characteristics we calculate partial residual functions in the same way as was described above.

Joint inversion of surface wave amplitude spectra and P wave polarities

Calculating radiation pattern of P waves for every current combination of parameters we compare it with observed polarities. The misfit obtained from this comparison we use to calculate a joint residual of surface wave amplitude spectra and polarities of P wave first arrivals. Let $\varepsilon_{\mathrm{amp}}$ be the residual of surface wave amplitude spectra, ε_{p} - the residual of P wave first arrival polarities (the number of wrong polarities divided by the full number of observed polarities), then we determine the joint residual ε by formula

$$\varepsilon = 1 - (1 - \varepsilon_{\mathrm{p}})(1 - \varepsilon_{\mathrm{amp}}). \qquad (2.5)$$

For this type of inversion we calculate partial residual functions to characterize the resolution of parameters under determination in the same way as it was described for two first types.

Before inversion we apply to observed polarities a smoothing procedure (see Lasserre *et al.*, 2001), which we will describe here briefly.

Let us consider a group of observed polarities (+1 for compression and -1 for dilatation) radiated in directions deviating from any medium one by a small angle. This group is presented in the inversion procedure by one polarity prescribing to this medium direction. If the number of one of two types of polarities from this group is significantly larger then the number of opposite polarities, then we prescribe this polarity to this medium direction. If no one of two polarity types can be considered as preferable, then all these polarities will not be used in the inversion. To make a decision for any group of n observed polarities we calculate the sum $m = n_+ - n_-$, where n_+ is the number of compressions and $n_- = n - n_+$ is the number of dilatations. We consider one of polarity types as preferable if $|m|$ is larger then its standard deviation in the case when +1 and -1 appear randomly with this same probability 0.5. In this case n_+ is a random value distributed following the binomial low. For its average we have $M(n_+) = 0.5n$, and for dispersion $D(n_+) = 0.25n$. Random value m is a linear function of n_+ such that $m = 2n_+ - n$. So following equations are valid for the average, for the dispersion, and for the standard deviation σ of value m

$M(m) = 2M(n_+) - n = n - n = 0$, $D(m) = 4D(n_+) = n$, and $\sigma(m) = \sqrt{n}$.

As a result, if the inequality $|m| \geq \sqrt{n}$ is valid then we prescribe +1 to the medium direction if $m > 0$, and -1 if $m < 0$.

Example of application

We illustrate the technique by results of its application for a study of January 22, 2003 Colima, Mexico, Earthquake, M_w=7.4. Using frequency-time and polarization analysis programs (see Lander, 1989) we analyzed fundamental Love and Rayleigh modes recorded by worldwide seismic networks. We selected for moment tensor and source depth inversion records of 14 stations. We used the signals of a good quality and normal polarization. The distribution of selected stations with respect to the epicenter is given in figure 2.

Analyzing the long period part of the spectra (periods from 100 to 250 seconds) we determined the following focal mechanism of the source: strike 300°, dip 15°, and rake -90°. The seismic moment estimate is equal to $0.18 \cdot 10^{21}$N·m. The four equivalent solutions obtained by inversion of amplitude surface wave spectra are presented in figure 3. The procedure of polarity smoothing is illustrated by figure 4 (the value of angle was taken equal to 10º). The focal mechanism obtained by joint inversion of surface wave amplitude spectra and first arrival polarities is shown in figure 5. In the same figure we show the polarities of first arrivals. As can be seen from comparison of figures 3 and 5 the last solution does not differ from one of four equivalent solutions obtained by inversion of amplitude surface wave spectra.

The source depth is imperfectly resolved because of low sensitivity of very long surface wave spectra to relatively small changes of source depth. The residual function for the source depth is given in figure 6. Our estimate of depth is 28 km.

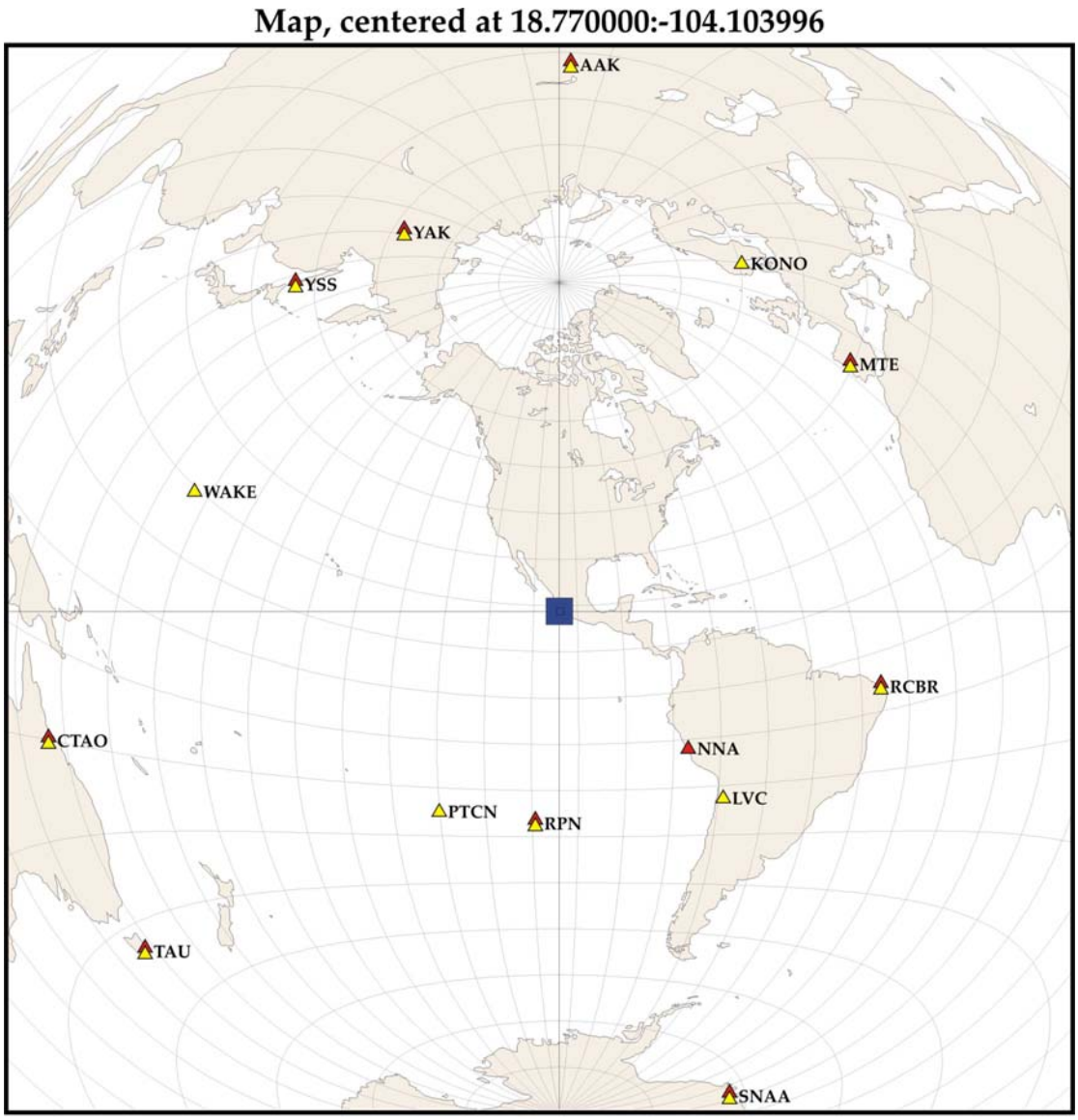

Figure 2. Distribution of stations used for moment tensor inversion
▲ - Love waves used for the inversion
△ - Rayleigh waves used for the inversion

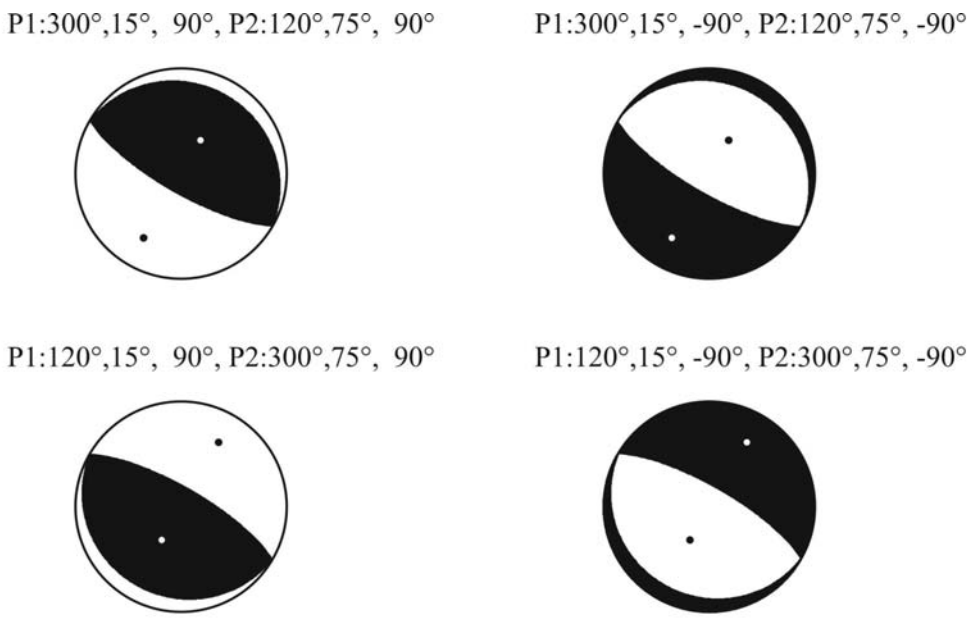

Figure 3. Four equivalent best solutions obtained by surface wave amplitude spectra inversion.

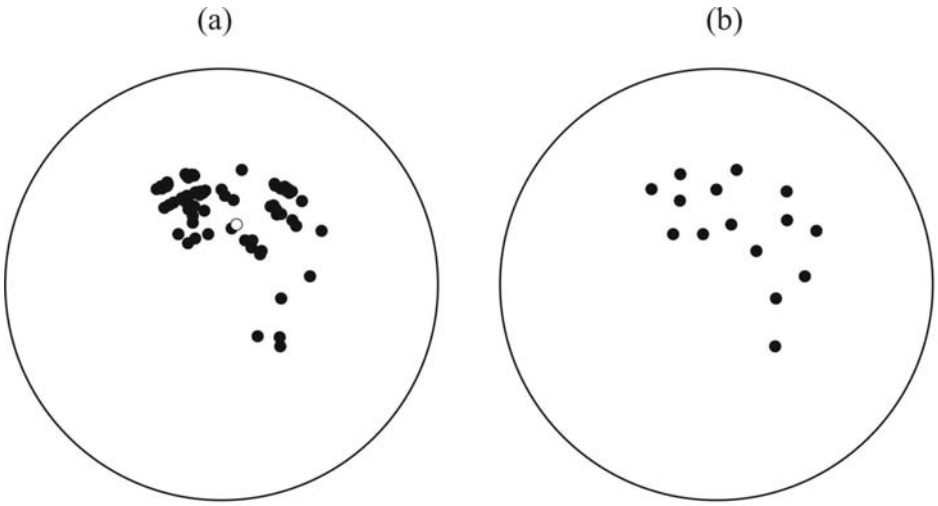

Figure 4. (a) Original and (b) selected and rarefied first arrival polarities.

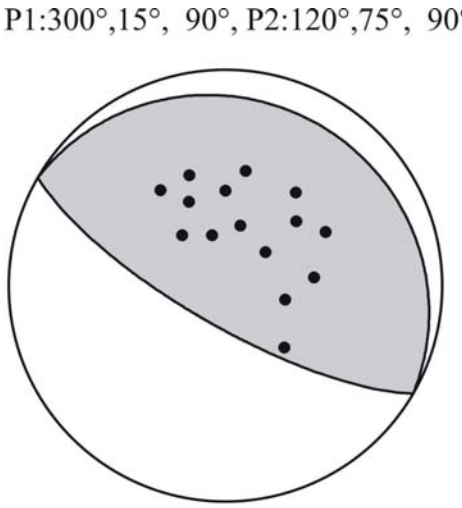

Figure 5. Best double couple obtained by joint inversion of surface wave amplitude spectra and first arrival polarities.

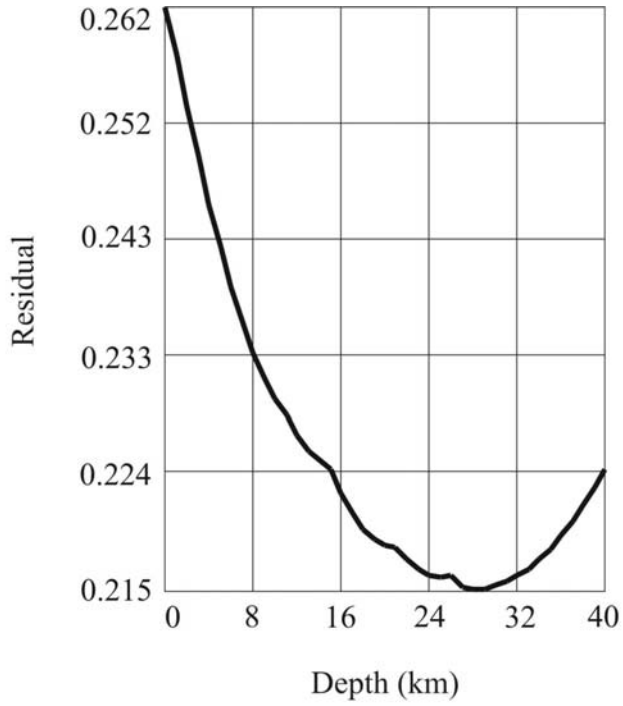

Figure 6. Residual function as for source depth obtained by joint inversion of surface wave amplitude spectra and P-wave polarities.

III. Second moments approximation. Characteristics of source shape and evolution in time.

We present here a technique based on the description of seismic source distribution in space and in time by integral moments (see Bukchin *et al.*, 1994; Bukchin, 1995; Gomez, 1997 a, b). We assume that the time derivative of stress glut tensor $\dot{\Gamma}$ can be represented in form (1.20). Following Backus and Mulcahy, 1976 we will define the source region by the condition that function $f(\mathbf{x},t)$ is not identically zero and the source duration is the time during which nonelastic motion occurs at various points within the source region, i.e., $f(\mathbf{x},t)$ is different from zero.

Spatial and temporal integral characteristics of the source can be expressed by corresponding moments of the function $f(\mathbf{x},t)$ (Backus, 1977a; Bukchin *et al.*, 1994). These moments can be estimated from the seismic records using the relation between them and the displacements in seismic waves, which we will consider later. In general case stress glut rate moments of spatial degree 2 and higher are not uniquely determined by the displacement field (Pavlov, 1994; Das & Kostrov, 1997). But in the case when equation (1.20) is valid such uniqueness takes place (Backus, 1977b; Bukchin, 1995).

Following equations define the spatio-temporal moments of function $f(\mathbf{x},t)$ of total degree (both in space and time) 0, 1, and 2 with respect to point $\mathbf{q}$ and instant of time τ.

$$f^{(0,0)} = \int_V dV \int_0^\infty f(\mathbf{x},t)dt\,, \quad f_i^{(1,0)}(\mathbf{q}) = \int_V dV \int_0^\infty f(\mathbf{x},t)(x_i - q_i)dt\,,$$

$$f^{(0,1)}(\tau) = \int_V dV \int_0^\infty f(\mathbf{x},t)(t-\tau)dt\,, \quad f^{(0,2)}(\tau) = \int_V dV \int_0^\infty f(\mathbf{x},t)(t-\tau)^2 dt\,,$$

$$f_i^{(1,1)}(\mathbf{q},\tau) = \int_V dV \int_0^\infty f(\mathbf{x},t)(x_i - q_i)(t-\tau)dt\,, \tag{3.1}$$

$$f_{ij}^{(2,0)}(\mathbf{q}) = \int_V dV \int_0^\infty f(\mathbf{x},t)(x_i - q_i)(x_j - q_j)dt$$

Using these moments we will define integral characteristics of the source. Source location is estimated by the spatial centroid $\mathbf{q}_c$ of the field $f(\mathbf{x},t)$ defined as

$$\mathbf{q}_c = \mathbf{f}^{(1,0)}(\mathbf{0}) / M_0\,, \tag{3.2}$$

where $M_0 = f^{(0,0)}$ is the scalar seismic moment.

Similarly, the temporal centroid τ_c is estimated by the formula

$$\tau_c = f^{(0,1)}(0) / M_0\,. \tag{3.3}$$

The source duration is Δt estimated by $2\Delta\tau$, where

$$(\Delta\tau)^2 = f^{(0,2)}(\tau_c) / M_0\,. \tag{3.4}$$

The spatial extent of the source is described by matrix $\mathbf{W}$,

$$\mathbf{W} = \mathbf{f}^{(2,0)}(\mathbf{q}_c) / M_0\,. \tag{3.5}$$

The mean source size in the direction of unit vector $\mathbf{r}$ is estimated by value $2l_r$, defined by formula

$$l_r^2 = \mathbf{r}^{\mathrm{T}}\mathbf{W}\mathbf{r}\,, \tag{3.6}$$

where $\mathbf{r}^{\mathrm{T}}$ is the transposed vector. From (3.5) and (3.6) we can estimate the principal axes of the source. There directions are given by the eigenvectors of the matrix $\mathbf{W}$, and the lengths are defined by correspondent eigenvalues: the length of the minor semi-axis is equal to the least eigenvalue, and the length of the major semi-axis is equal to the greatest eigenvalue.

In the same way, from the coupled space time moment of order (1,1) the mean velocity **v** of the instant spatial centroid (Bukchin, 1989) is estimated as

$$\mathbf{v} = \mathbf{w} / (\Delta\tau)^2 \ , \qquad (3.7)$$

where $\mathbf{w} = \mathbf{f}^{(1,1)}(\mathbf{q}_c, \tau_c) / M_0$.

Now we will consider the low frequency part of the spectra of the i^{th} component of displacements in Love or Rayleigh wave $u_i(\mathbf{x},\omega)$. It is assumed that the frequency ω is small, so that the duration of the source is small in comparison with the period of the wave, and the source size is small as compared with the wavelength. It is assumed that the origin of coordinate system is located in the point of spatial centroid $\mathbf{q}_c$ (i.e. $\mathbf{q}_c = \mathbf{0}$) and that time is measured from the instant of temporal centroid, so that $\tau_c = 0$. With this choice the first degree moments with respect to the spatial origin **x=0** and to the temporal origin t=0 are zero, i.e. $\mathbf{f}^{(1,0)}(\mathbf{0}) = \mathbf{0}$ and $f^{(0,1)}(0) = 0$.

Under this assumptions, taking into account in formula (1.23) only the first terms for $l + n \le 2$ we can express the relation between the spectrum of displacements $u_i(\mathbf{x},\omega)$ and the spatio-temporal moments of the function $f(\mathbf{x},t)$ by following formula (Bukchin,1995)

$$u_i(\mathbf{x},\omega) = \frac{1}{\mathrm{i}\omega} M_0 M_{jl} \frac{\partial}{\partial y_l} G_{ij}(\mathbf{x},\mathbf{0},\omega) + \frac{1}{2\,\mathrm{i}\omega} f^{(2,0)}_{mn}(\mathbf{0}) M_{jl} \frac{\partial}{\partial y_m}\frac{\partial}{\partial y_n}\frac{\partial}{\partial y_l} G_{ij}(\mathbf{x},\mathbf{0},\omega)$$

$$- f^{(1,1)}_{m}(\mathbf{0},0) M_{jl} \frac{\partial}{\partial y_m}\frac{\partial}{\partial y_l} G_{ij}(\mathbf{x},\mathbf{0},\omega) + \frac{\mathrm{i}\omega}{2} f^{(0,2)}(0) M_{jl} \frac{\partial}{\partial y_l} G_{ij}(\mathbf{x},\mathbf{0},\omega) \ , \qquad (3.8)$$

i,j,l,m,n = 1,2,3 and the summation convention for repeated subscripts is used. $G_{ij}(\mathbf{x},\mathbf{y},\omega)$ in equation (3.8) is the spectrum of Green function for the chosen model of medium and wave type. We assume that the paths from the earthquake source to seismic stations are well approximated by weak laterally inhomogeneous model. Under this assumption, as it was mentioned above, the amplitude spectrum $|u_i(\mathbf{x},\omega)|$ defined by formula (3.8) does not depend on the average phase velocity of the wave, and the errors in source location do not affect the amplitude spectrum.

If all characteristics of the medium, depth of the best point source and seismic moment tensor are known (determined, for example, using the spectral domain of longer periods) the representation (3.8) gives us a system of linear equations for moments of the function $f(\mathbf{x},t)$ of total degree 2. But as we mentioned considering moment tensor approximation the average phase velocities of surface waves are usually not well known. For this reason, we use only amplitude spectrum of surface waves for determining these moments, in spite of non-linear relation between them.

Let us consider a plane source. All moments of the function $f(\mathbf{x},t)$ of total degree 2 can be expressed in this case by formulas (3.2)-(3.7) in terms of 6 parameters: Δt - estimate of source duration, $l_{\max}$ - estimate of maximal mean size of the source, φ_l - estimate of the angle between the direction of maximal size and strike axis, $l_{\min}$ - estimate of minimal mean size of the source, v - estimate of the absolute value of instant centroid mean velocity **v** and φ_v - the angle between **v** and strike axis.

Using the Bessel inequality for the moments under discussion we can obtain the following constrain for the parameters considered above (Bukchin, 1995):

$$v^2 \Delta t^2 \left(\frac{\cos^2\varphi}{l^2_{\max}} + \frac{\sin^2\varphi}{l^2_{\min}} \right) \le 1 \ , \qquad (3.9)$$

where φ is the angle between major axis of the source and direction of **v**.

Assuming that the source is a plane fault and representation (1.20) is valid let us consider a rough grid in the space of 6 parameters defined above. These parameters have to follow

inequality (3.9). Let models of the media be given and the moment tensor be fixed as well as the depth of the best point source. Let the fault plane (one of two nodal planes) be identified. Using formula (3.8) we can calculate the amplitude spectra of surface waves at the points of observation for every possible combination of values of the varying parameters. Comparison of calculated and observed amplitude spectra give us a residual $\varepsilon^{(i)}$ for every point of observation, every wave and every frequency ω. Let $u^{(i)}(\mathbf{r},\omega)$ be any observed value of the spectrum, i = 1,…,N; $\varepsilon^{(i)}$ - corresponding residual of $|u^{(i)}(\mathbf{r},\omega)|$. We define the normalized amplitude residual by formula

$$\varepsilon(\Delta t, l_{\max}, l_{\min}, \varphi_l, v, \varphi_v) = \left[\left(\sum_{i=1}^{N} \varepsilon^{(i)2}\right) \Big/ \left(\sum_{i=1}^{N} |u^{(i)}(\mathbf{r},\omega|^2\right)\right]^{1/2} . \quad (3.10)$$

The optimal values of the parameters that minimize ε we consider as estimates of these parameters. We search them by a systematic exploration of the six dimensional parameter space. To characterize the degree of resolution of every of these source characteristics we calculate partial residual functions in the same way as was described in previous section. We define 6 functions of the residual corresponding to the 6 varying parameters: $\varepsilon_{\Delta t}(\Delta t)$, $\varepsilon_{l_{\max}}(l_{\max})$, $\varepsilon_{l_{\min}}(l_{\min})$, $\varepsilon_{\varphi_l}(\varphi_l)$, $\varepsilon_v(v)$ and $\varepsilon_{\varphi_v}(\varphi_v)$. The value of the parameter for which the corresponding function of the residual attains its minimum we define as estimate of this parameter. At the same time these functions characterize the degree of resolution of the corresponding parameters.

Example of application

We illustrate the technique by results of its application for a study of the same Colima earthquake, which we considered above.

To estimate duration and geometry of the source we have used amplitude spectra of fundamental modes of Love and Rayleigh waves in the spectral domain from 50 to 100 seconds. We selected 11 Love wave records and 9 Rayleigh wave records from FDSN stations. Their azimuthal distribution is shown in figure 7.

We fixed source depth (28km), focal mechanism and seismic moment obtained from analysis of long period surface wave spectra considered above. The nodal plane dipping to the Northeast was identified as a fault plane.

The inversion (figure 8) yields a characteristic duration of 10 s, a characteristic source length of 50 km. The minor ellipse axis length, i,e, the characteristic width, is poorly resolved, lying between 0 and 20 km. The average instant centroid velocity estimate is about 3 km/s. The angles giving the ellipse and velocity vector orientations are measured clockwise on the foot wall starting from the strike axis. They are consistent with each other and correspondent residual functions, calculated while all other parameters were fixed to their optimum values, attain their minimum values at 105°.

The propagation of rupture may be characterized by directivity ratio *d* proposed by McGuire *et al*. (2002). This parameter is defined as the ratio of the average velocity of the instant centroid over the apparent rupture velocity equal to $l_{\max}/\Delta t$. For a unilateral rupture where slip nucleates at one end of a rectangular fault and propagates to the other at a uniform rupture velocity with a uniform slip distribution, d = 1. However, for a symmetric bilateral rupture that initiates in the middle and propagates to both ends of a fault at uniform rupture velocity with uniform slip distribution, d = 0. Predominantly bilateral ruptures correspond to $0 \le d < 0.5$ while predominantly unilateral ruptures correspond to $0.5 < d \le 1$. We find d = 0.6 for our model. This value shows that unilateral (northward) rupture propagation is slightly preferred.

We compared our estimate of source duration with similar integral estimate calculated as second moment of moment-rate function (see figure 9), calculated by Yagi (Home Page, 2003). The value obtained for this estimate is equal to 10.5 s, which is very close to our estimate of source duration.
The source model characterized by considered integral estimates is schematically represented in figure 10.

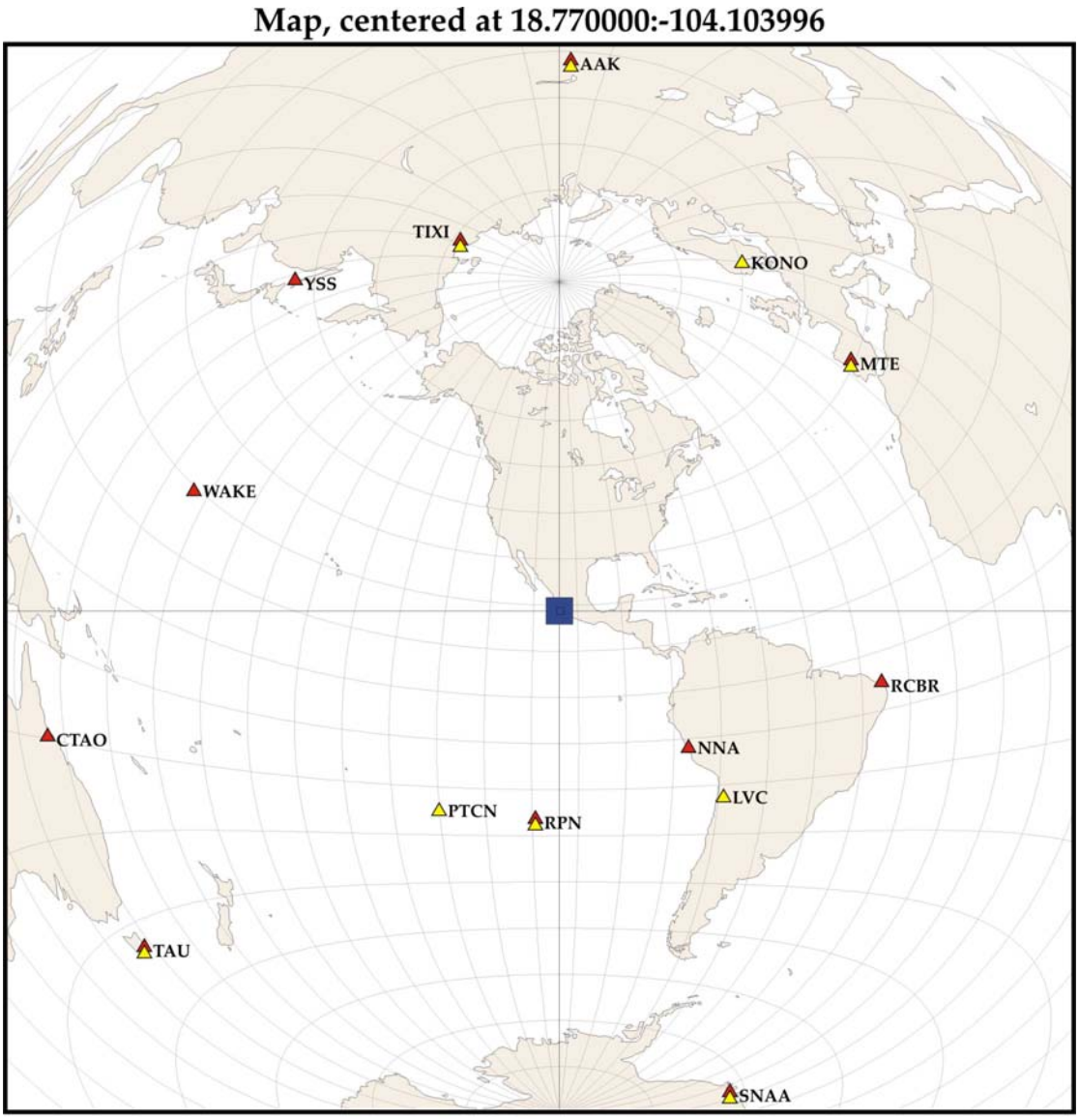

Figure 7. Distribution of stations used for 2-nd moments inversion, similar to that used for moment tensor inversion.
▲ - Love waves used for the inversion
△ - Rayleigh waves used for the inversion

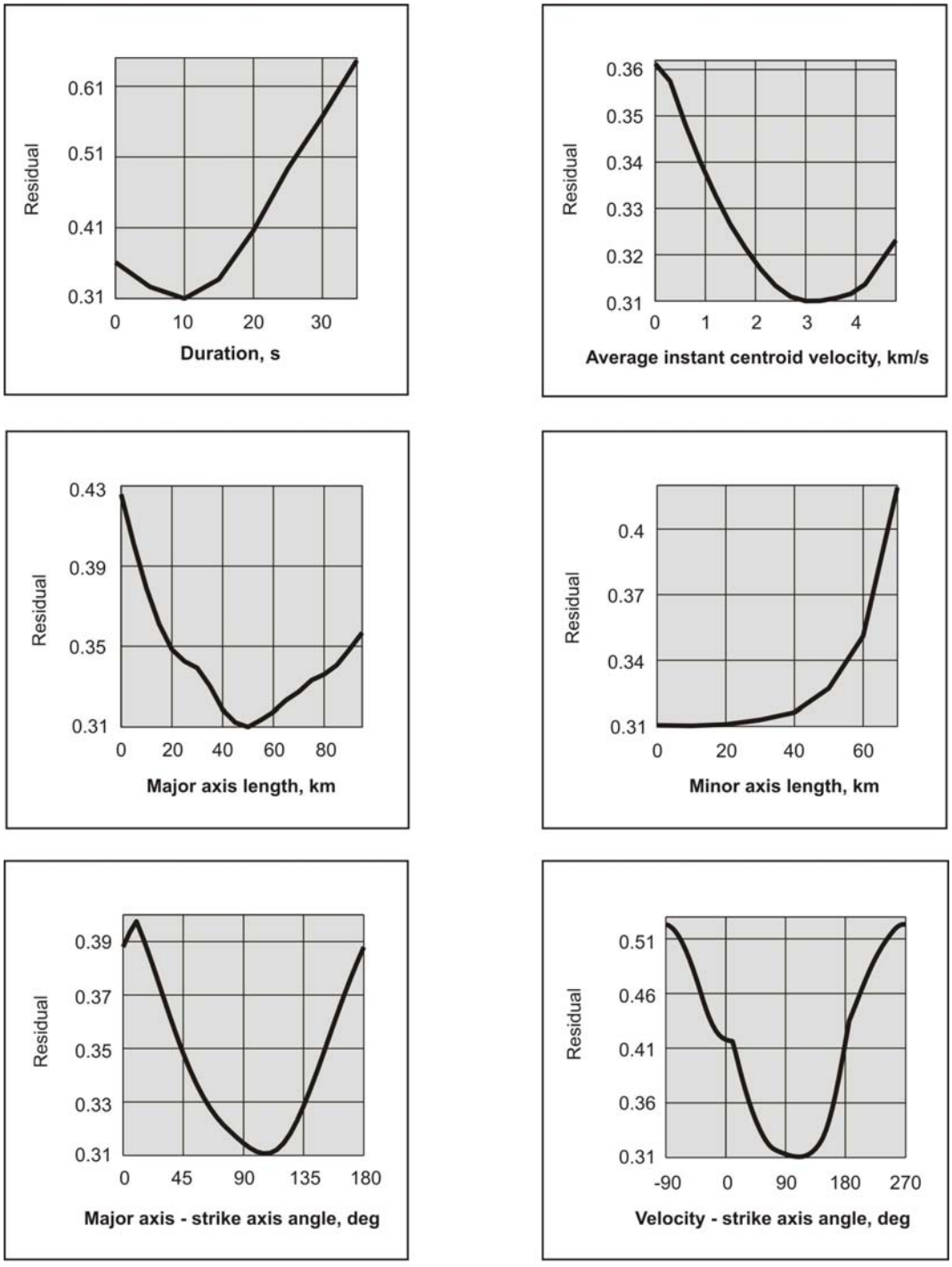

Figure 8. Integral estimates of source characteristics from 50-100 s surface wave amplitude spectra analysis.

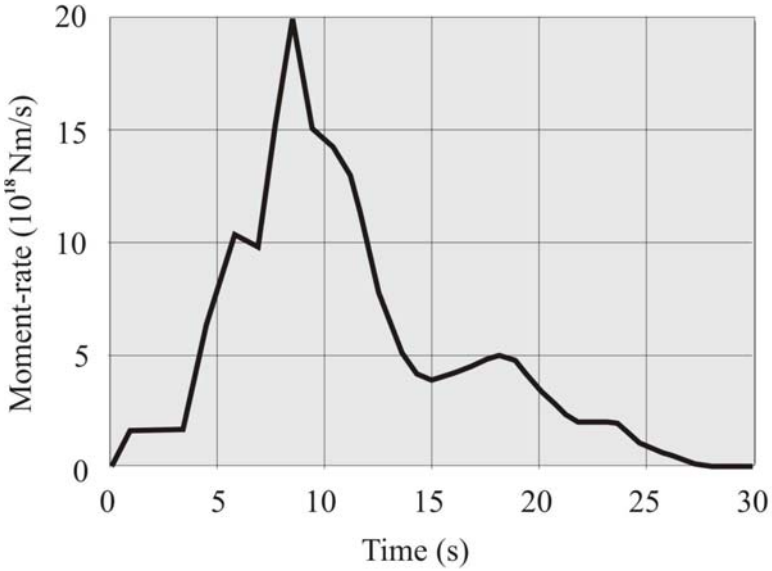

Figure 9. Moment rate function (Yagi@IISEE, BRI, 2003)

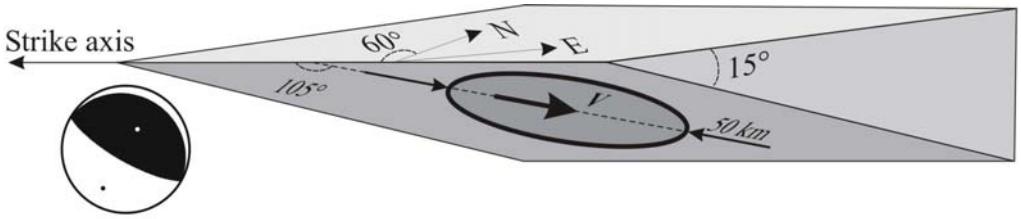

Figure 10. Focal mechanism and scheme of the source model. Ellipse represents the integral estimates of source geometry. **V** - direction of instant centroid velocity.

IV. Surface wave focusing

As it was mentioned above, calculating surface wave Green function we assume that waves propagate along great circles. Practically all applications related to surface wave interpretation are based on this assumption. At the same time it is known from tomography studies that lateral variations of surface wave phase velocity can attain 10%. These variations can cause significant deviation of wave traces from great circles and related to it anomalies of geometrical spreading (focusing effects).

A numerical modeling of these effects was performed in collaboration with T.Yanovskaya, A.Mostinsky, J.-P. Montagner, and E. Beucler. The modeling is based on a new technique for kinematic ray tracing and dynamic ray tracing on a spherical surface, developed by T.Yanovskaya. We will not consider the technique in this lecture. We will show examples of its application and results of comparison of predicted and observed amplitude anomalies related to surface wave focusing.

For a given map of phase velocity anomalies and location of earthquake epicenter we perform ray tracing for any location of receiver or for a greed covering the Earth surface.

Using this technique and recent global phase velocity maps we calculate spectral anomalies for fundamental Rayleigh mode in the period range from 60 to 150 seconds.

Observed surface wave spectra depend on elastic model of the Earth and on its anelastic model, determining the wave attenuation. Deviation of these two models from spherical symmetry effect on wave amplitude spectra. We compare these two effects.

We analyze the fitting between calculated and observed focusing effects using records of the earthquakes occurred in different seismic regions with magnitude M_s varying from 6 to 7 (over 3000 measurements).

Calculation of surface wave spectra

As it was mentioned above we approximate the elastic model of the Earth by a weak laterally inhomogeneous model. The spectrum of displacements $\mathbf{u}(\omega)$ in surface wave generated by an instant point source in such a model (Levshin *et al.*, 1989) can be expressed in form

$$\mathbf{u}(\mathbf{x}_r,\omega) = \frac{\exp(-i\pi/4)}{\sqrt{8\pi}} \frac{\exp(-i\omega\tau)}{\sqrt{\omega J/c}} \frac{\chi(\mathbf{x}_s,\gamma,\omega)}{\sqrt{cvI}\Big|_s} \frac{\mathbf{U}(\mathbf{x}_r,\omega)}{\sqrt{cvI}\Big|_r} q(\mathbf{x}_r,\omega)\,. \qquad (3.1)$$

Here ω is the angular frequency; $\mathbf{x}_s$ and $\mathbf{x}_r$ are the coordinates of the source and of the registration point; γ is the ray azimuth in the source; c and v – phase and group velocity of the wave; χ is the radiation pattern of the source dependent on the moment tensor, eigen functions and their derivatives in the source vicinity, and direction of radiation; $\mathbf{U}$ is the eigen function describing the distribution of displacements in the wave along the vertical direction; q is a factor describing the wave attenuation; I is the energy integral of eigen function; s and r are the indexes of the source and receiver correspondently; J is the geometrical spreading; τ is the wave arrival time. So, the surface wave spectrum in this approximation is determined by the near source and near receiver velocity structure, by the averaged along the wave path phase velocity and attenuation, and by geometrical spreading. For spherical symmetric Earth model we have $\tau = R\Delta/c_0$, $q = \exp[-\omega Q_0^{-1} R\Delta/(2c_0)]$, $J = R\sin\Delta$. Here R is the Earth radius, Δ is the epicentral distance, c_0 is the value of phase velocity of the wave, and Q_0^{-1} is the attenuation coefficient. In the case of laterally inhomogeneous medium we calculate the arrival time, attenuation and geometrical spreading of the wave integrating the systems of equations for ray tracing.

Numerical modeling of wave field anomalies

We perform numerical modeling of the effects due to lateral inhomogeneity of the elastic Earth model using global phase velocity anomaly maps for fundamental Rayleigh mode in the period range from 60 to 150 seconds (Beucler, 2002). An example of such a map for period 75 seconds is given in figure 11. The map is constructed in azimuthal equidistant projection for two hemispheres. The velocity anomalies errors are measured in percentage to the reference velocity value for spherically symmetric model PREM.

For any location of earthquake epicenter we perform ray tracing for any location of receiver or for a set of rays covering the Earth surface.

An example of a scheme of rays for fundamental Rayleigh mode for period 75 seconds is presented in figure 12. The epicenter is located in Indonesia. The rays are drawn in azimuthal equidistant projection. The deviations of rays from great circle arcs are small at distances not exceeding 90°, therefore the rays are shown for hemisphere centered at the epicenter's antipode ($90° < \Delta < 180°$), where these deviations become significant. As can be seen from the figure a multipathing area bounded by caustics appears in the vicinity of epicenter's antipode and even at large distances from antipode. Geometrical spreading is vanishing at the point where ray touches a caustic, and becomes negative after the tangency point. Numerical calculations show that among the rays passing any point of multipathing area there is at least one ray that has touched a caustic. These features of ray field are determined not only by lateral inhomogeneity of the Earth but also by the fact that rays are propagating on a sphere.

We measure amplitude anomaly caused by ray deviation from great circle arc by focusing coefficient *f*, defined as ratio of spectral amplitude in the case of lateral inhomogeneous Earth model and spectral amplitude of the same wave for correspondent spherically symmetric model. As it follows from formula (1) the value of f can be calculated by formula $f = \sqrt{\sin\Delta / J}$, where geometrical spreading *J* is calculated by dynamic ray tracing.

The amplitude anomaly map correspondent to the scheme of rays for fundamental Rayleigh mode for period 75 seconds considered above is represented in figure 13. The map is constructed in azimuthal equidistant projection for two hemispheres centered at the epicenter and at the epicenter's antipode. The amplitude anomalies are calculated at the rays covering the entire Earth surface except the multipathing area that is shaded gray. As can be seen from the figure generally sufficiently strong anomalies appear at epicentral distances $\Delta > 90°$. But they can be significant at shorter distances as well.

Effects of aspherical elastic and anelastic models on surface wave amplitude spectra

Deviation from spherical symmetry of anelastic model, determining the wave attenuation, effects on surface wave amplitude spectra as well as lateral inhomogeneity of velocity structure. We measure correspondent amplitude anomaly by relative q factor, defined similarly to focusing coefficient as ratio of spectral amplitude in the case of aspherical anelastic model and spectral amplitude of the same wave for correspondent spherically symmetric model. Its value is equal to the ratio of values of factor q in formula (1) calculated by integrating along the ray for two mentioned models.

We compare these amplitude anomalies with anomalies caused by rays focusing for fundamental Rayleigh mode at period 150 seconds. We use global map of local attenuation (Romanowicz, 1995) given by spherical harmonics expansion of order 10.

We selected 25 seismofocal zones from all over the world (see figure 14). Considering every zone as epicenter we calculated both effects for 250 locations of stations of the worldwide seismic network, in all 6138 traces. If the station was found in a multipathing area it was rejected from the consideration. The results of comparison of effects under consideration are represented by 2D diagram for relative q factor and focusing coefficient in figure 15. Every circle at the diagram corresponds to one of traces. As can be seen from the

figure the focusing effect caused by lateral inhomogeneity of the elastic Earth model can be significantly larger than the effect related to the lateral inhomogeneity of attenuation model, which does not exceed 20% for fundamental Rayleigh mode at period 150 seconds. Relying on this observation and since global aspherical models for Rayleigh wave attenuation for periods shorter than 100 seconds are not available we use in following analysis Q^{-1} values given by spherically symmetric model PREM.

Comparison of predicted focusing effect with observations

We performed the comparison of predicted and observed amplitude anomalies in fundamental Rayleigh wave using broadband records of 106 earthquakes ($6 < M_S < 7$) located in 25 seismic zones presented in figure 14. Using frequency-time analysis technique and floating filtering (Levshin *et al.*, 1989) we isolated fundamental Rayleigh mode for about 1400 traces. We don't consider signals recorded within the multipathing area or at distances from caustic exceeding one and a half of wavelength. We use records of a good quality, with significant signal to noise ratio and normal polarization in period range from 60 to 150 seconds. We calculated amplitude spectrum for periods 60, 75, 100 and 150 seconds for all filtered records. The spectra were corrected for the instrument response. Calculating synthetic spectra by formula (1) we used normalized moment tensors given by CMT solutions from Harvard catalog, and recalculated seismic moments from analyzing records. The structure models in source and station vicinities were given by 3SMAC model (Ricard *at al*., 1996). For every observed value of amplitude spectra we calculate two synthetic values: one is calculated taking into account the focusing effect, and another one – without taking it into account. Analyzing the fitting of these two synthetic spectra with observed spectral amplitudes we try to find if taking into account the focusing effect reduces the misfit significantly. We calculate the focusing coefficient f by shooting, integrating the ray tracing systems. At one time with focusing coefficient f we calculate the average along the ray values of errors of velocity anomalies determination β, which characterize the reliability of f estimate.

Data sampling

The total number of selected measurements is equal to 3256. We consider different samples of observations and correspondent synthetics according to the value of focusing coefficient f and to the value of average error β. Along with samples containing traces characterized by any value of f from its entire range we consider correspondent samples containing traces characterized by strong focusing effect ($f > 1.25$ or $f < 0.75$). Characterizing traces for every of concerned periods by error ratio $r = \beta / \beta_{max}$ where β_{max} is the maximum value of error β for this period, we consider samples with different value of r measured in percents.

The size of different samples for entire range of focusing effect is shown in table 1, and for traces with strong focusing effect – in table 2.

Period	$r \leq 100$	$r \leq 80$	$r \leq 60$	$r \leq 40$	$r \leq 20$
Mix of 4 perio	3256	3171	2504	1370	431
60s	802	777	573	277	50
75s	895	873	690	327	65
100s	872	848	666	398	147
150s	687	679	575	368	169

Table1. Data sampling with respect to the error of velocity anomalies determination for entire range of focusing effect.

Period	$r \le 100$	$r \le 80$	$r \le 60$	$r \le 40$	$r \le 20$
Mix of 4 perio	786	751	564	259	72
60s	263	251	168	78	15
75s	276	263	208	77	15
100s	167	157	122	61	23
150s	80	80	66	43	19

Table2. Data sampling with respect to the error of velocity anomalies determination for strong focusing effect.

The distribution density of the number of measurements with respect to the value of focusing coefficient for different samples according to the error ratio *r* is shown in figure 16.

Characterizing the fitting between synthetic and observed amplitude spectra we consider relative misfit as well as absolute misfit.

Relative misfit

We characterize the fitting between synthetic and observed amplitude spectra by value $\xi = \ln(u_{syn} / u_{obs})$. Here u_{syn} is the value of synthetic amplitude spectra and u_{obs} is the value of observed amplitude spectra. In the case of ideal fitting ξ is vanishing. When the values of synthetic and observed amplitude spectra are close ξ coincides with the value of relative error of the theoretical estimate.

The histograms for ξ value calculated for different samples are presented in figure 17. In the case of ideal fitting between synthetic and observed amplitude spectra the ξ histogram should represent a delta function concentrated in zero. For every sample we show two histograms: one corresponds to synthetic amplitude spectra calculated taking into account the focusing effect, another one corresponds to synthetic amplitude spectra calculated without taking into account this effect. As one can see the improvement of fitting due to correction of spectra for focusing effect becomes remarkable when we consider the traces characterized by small enough error ratio *r*. Particularly it is clear for the sample correspondent to strong focusing effect.

We measure the fitting between synthetic and observed amplitude spectra by *rms* value of ξ defined by formula $s = \sqrt{\sum_{i=1}^{N} \xi_i^2 / N}$, where *N* is the number of observations. In the case of ideal fitting *s* is vanishing. Let s_0 be the *s* value calculated without taking into account the focusing effect, and s_{corr} corresponds to synthetic amplitude spectra corrected for it. Then the reduction of misfit due to correction for focusing effect can be calculated as $\Delta s = s_0 - s_{corr}$. The ratio $\Delta s/s_0$ for the mix of four concerned periods and for every period separately is shown in figure 18. The ratio characterizing the reduction of misfit is given as a function of the upper boundary of the error ratio *r*. We present separately the results for samples correspondent to entire range of focusing effect and the results for traces with strong focusing effect.

Along with reduction of relative misfit we calculate its normalized value. Let $s_0 = \sqrt{\sum_{i=1}^{N} \xi_i^2 / N}$ corresponds to synthetic amplitude spectra calculated without taking into account the focusing effect. As it follows from formula (1) and from the definition of focusing coefficient *f* we have for corrected spectra

$$s_{corr} = \sqrt{\sum_{i=1}^{N} (\xi_i + \ln f_i)^2 / N}.$$

Let us introduce the following notation:

$$s_f = \sqrt{\sum_{i=1}^{N} (\ln f_i)^2 / N}.$$

It can be shown that following inequality is valid:

$\Delta s = s_0 - s_{corr} \le s_f$

We define the ratio $\Delta s / s_f$ as normalized reduction of misfit. The results for normalized reduction are presented in figure 19 in the same form as for reduction in figure 18. As one can see the values of normalized reduction for large samples correspondent to entire range of focusing effect and for relatively small samples with traces characterized by strong focusing effect are comparable. This fact makes the reduction estimates for strong focusing effect shown in figure 18 more reliable.

Absolute misfit – estimate1

Let ε_{q_i} and $\varepsilon_{q_{corr_i}}$ be the absolute misfit between synthetic and observed amplitude spectra for *i*-th measurement of *q*-th earthquake calculated without taking into account the focusing effect and taking it into account correspondingly. Let N_q be the number of such measurements, m_{0_q} - the seismic moment of the *q*-th earthquake, and $\langle m_0 \rangle$ - the earthquake-average value of seismic moment. We characterize the misfit for *q*-th earthquake by *rms* values of ε_{q_i} and $\varepsilon_{q_{corr_i}}$ normalized by seismic moment:

$$E_q = \frac{\langle m_0 \rangle}{m_{0_q}} \sqrt{\frac{\sum_{i=1}^{N_q} \varepsilon_{q_i}^2}{N_q}}, \qquad E_{q_{corr}} = \frac{\langle m_0 \rangle}{m_{0_q}} \sqrt{\frac{\sum_{i=1}^{N_q} \varepsilon_{q_{corr\,i}}^2}{N_q}}.$$

We define the earthquake-average reduction of absolute misfit as difference between these two values averaged over all earthquakes:

$$\Delta\langle E \rangle = \langle E \rangle - \langle E_{corr} \rangle.$$

The ratio $\Delta\langle E \rangle / \langle E \rangle$ for the mix of four concerned periods and for every period separately are shown in figure 20. Similarly to figures 18 and 19 the ratio characterizing the reduction of absolute misfit is given as a function of the upper boundary of the error ratio *r*.

Absolute misfit – estimate 2

We characterize the absolute misfit for any sample of data by *rms* value of misfits ε_{q_i} and $\varepsilon_{q_{corr_i}}$ considered in preceding paragraph, normalized by correspondent seismic moments. Let *L* be the number of earthquakes. We define the misfits calculated without taking into account the focusing effect and taking it into account by formulae

$$E = \sqrt{\frac{\sum_{q=1}^{L} \sum_{i=1}^{N_q} \frac{\langle m_0 \rangle^2}{m_{0_q}^2} \varepsilon_{q_i}^2}{\sum_{q=1}^{L} N_q}}, \quad E_{corr} = \sqrt{\frac{\sum_{q=1}^{L} \sum_{i=1}^{N_q} \frac{\langle m_0 \rangle^2}{m_{0_q}^2} \varepsilon_{q_{corr\,i}}^2}{\sum_{q=1}^{L} N_q}},$$

and the reduction of misfit by correspondent difference

$$\Delta E = E - E_{corr}.$$

The ratio $\Delta E/E$ for the mix of four concerned periods and for every period separately is shown in figure 21.

Discussion of results

As can be seen from presented results the reduction of misfit caused by taking into account the focusing effect predominantly grows up with decreasing of the maximum of the error ratio *r*. Such a sensitivity of fitting improvement to the averaged along ray pass accuracy of tomography maps is natural. For samples including traces characterized by any value of *r* (*r* < 100%) the reduction of misfit is vanishing or becomes even negative, what means increase of misfit. The improvement of fitting becomes considerable for traces characterized by strong focusing effect and small error ratio *r*.

The results obtained for different periods differ from each other visibly. The most significant improvement is achieved for periods 100s and 75 s. The magnitude of focusing effect is calculated using velocity anomaly maps. But the sampling of data related to the error ratio *r* is performed on the basis of maps for errors of velocity anomalies determination. So, the difference of results for different periods may reflect the different quality of both kinds of maps.

Conclusions

Presented results of numerical modeling and analysis of real seismic records show that synthetic and observed Rayleigh wave amplitude spectra are more similar if the focusing effect is taken into account. The improvement of the fit of synthetics to observations is sensitive to the averaged along ray pass accuracy of tomography maps. It is significant from practical point of view for traces with high average accuracy and strong focusing effect exceeding the errors due to other factors, such as lateral inhomogeneity of attenuation, errors of source parameters determination, scattering effects etc. Focusing effect should be taken into account in different applications, such as seismic source study, magnitude measurements, and Q estimation. Neglect of large anomalies of geometrical spreading, as well as stronger effects, such as caustics and multipathing, may lead to false estimates.

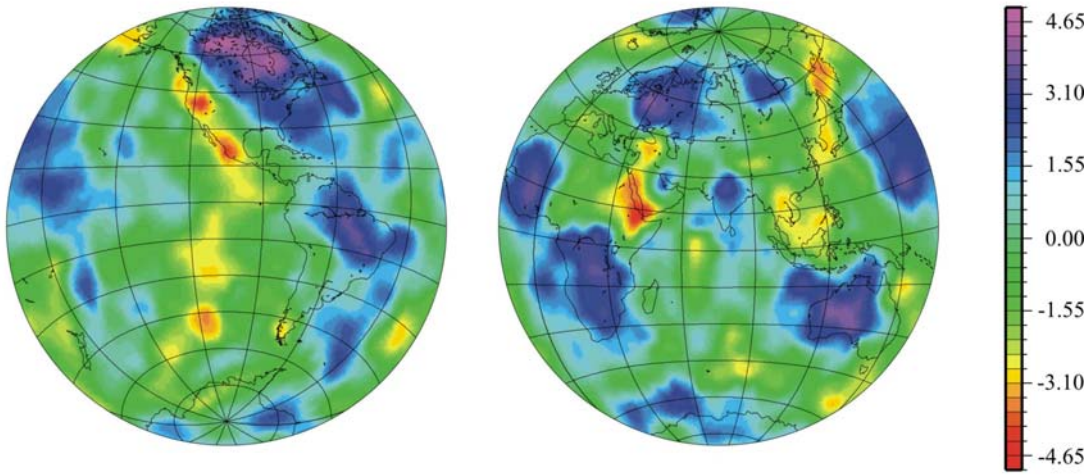

Figure 11. Phase velocity anomalies (%) for fundamental Rayleigh mode at period 75 s.

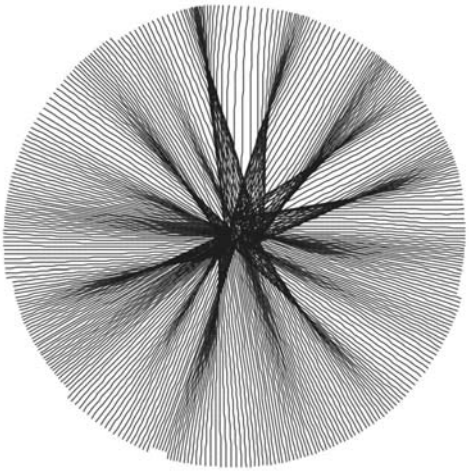

Figure 12. Scheme of rays for 75 s Rayleigh fundamental mode on hemisphere centered at the epicenter's antipode. The epicenter is located in Indonesia (-1°, 124°).

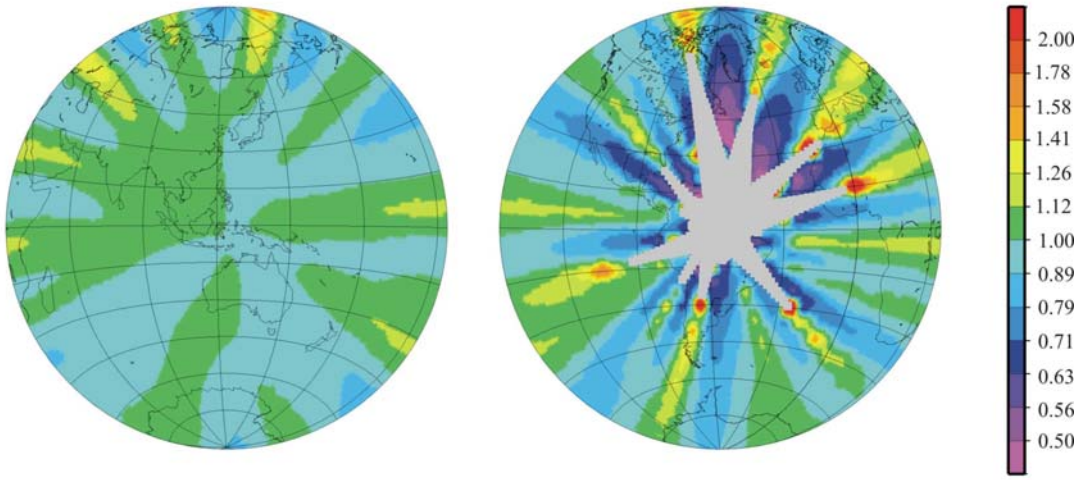

Figure 13. Map for amplitude anomalies for 75 s Rayleigh fundamental mode. The epicenter is located in Indonesia (-1°, 124°). Multipathing area is shaded gray.

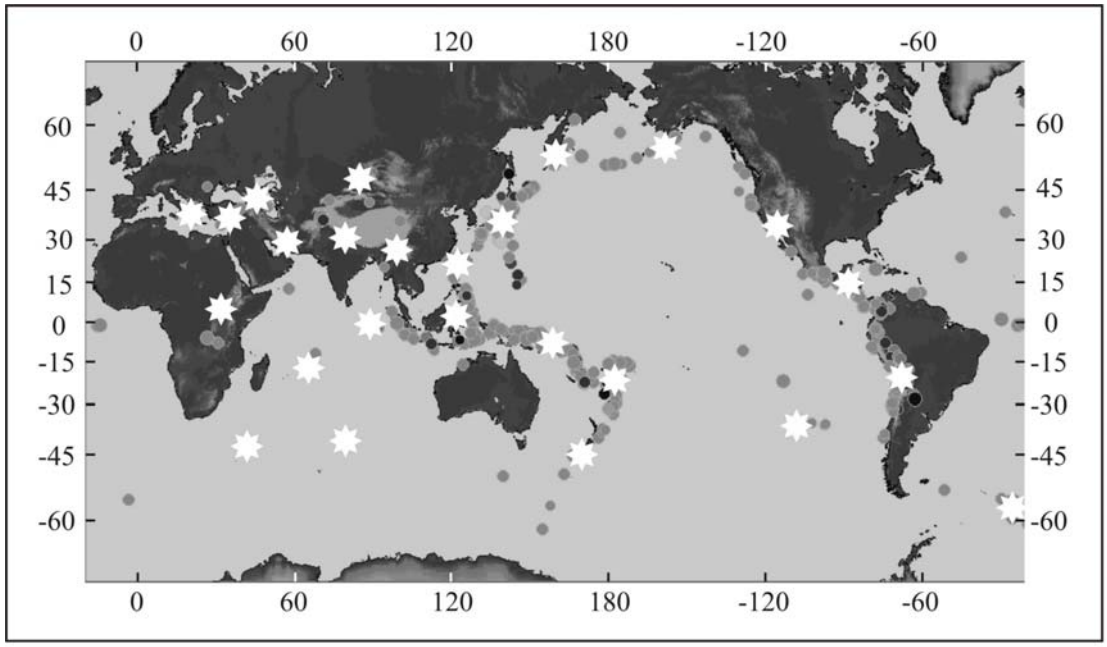

Figure 14. World seismicity ($6.5 < M_s < 7.0$) for period from 1990 to 2000 and focal zones (stars) selected for the study of effects related to the deviation from spherical symmetry of the elastic and anelastic Earth models.

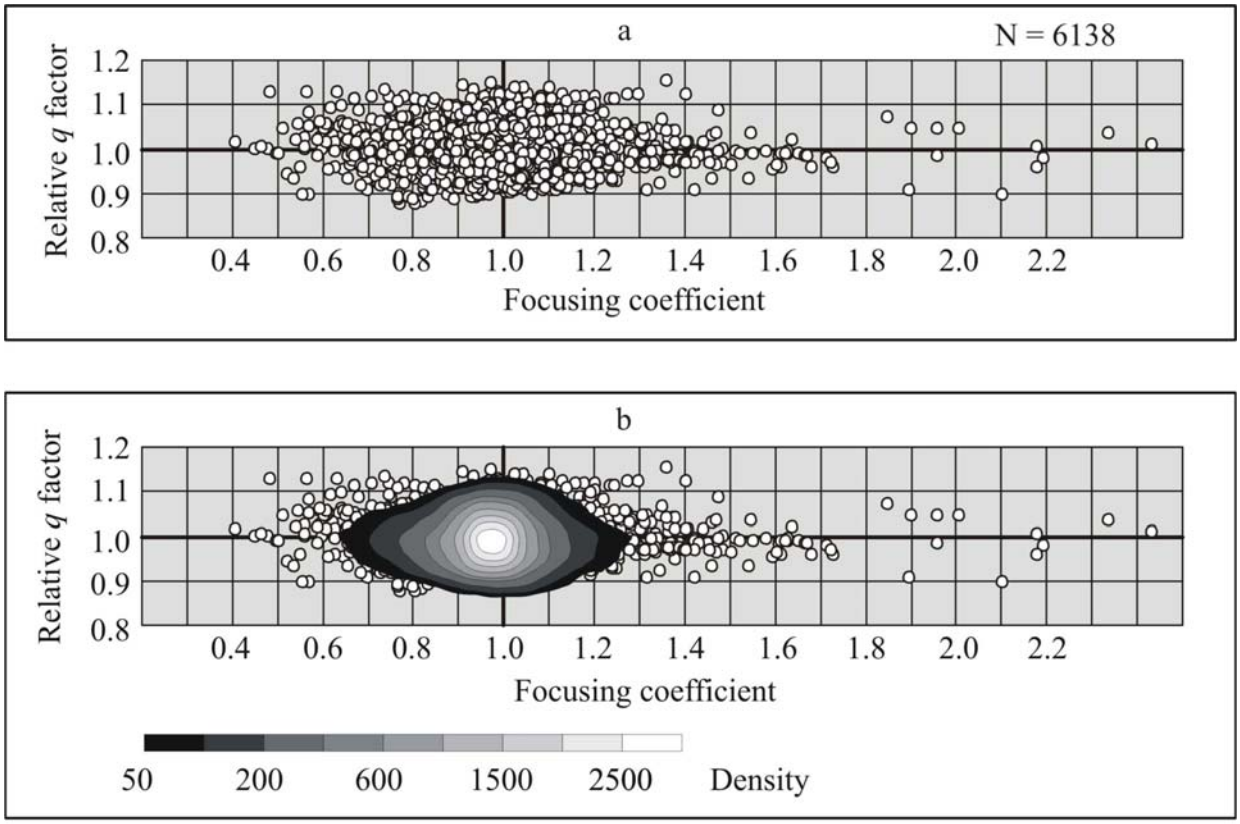

Figure 15. (a) Comparison of relative amplitude factors due to focusing effect and to inhomogeneity of attenuation for Rayleigh fundamental mode (T = 150 s). Every circle corresponds to one of traces. (b) The same diagram as (a), superimposed by a map for circles density (number of circles in a square 0.1×0.1).

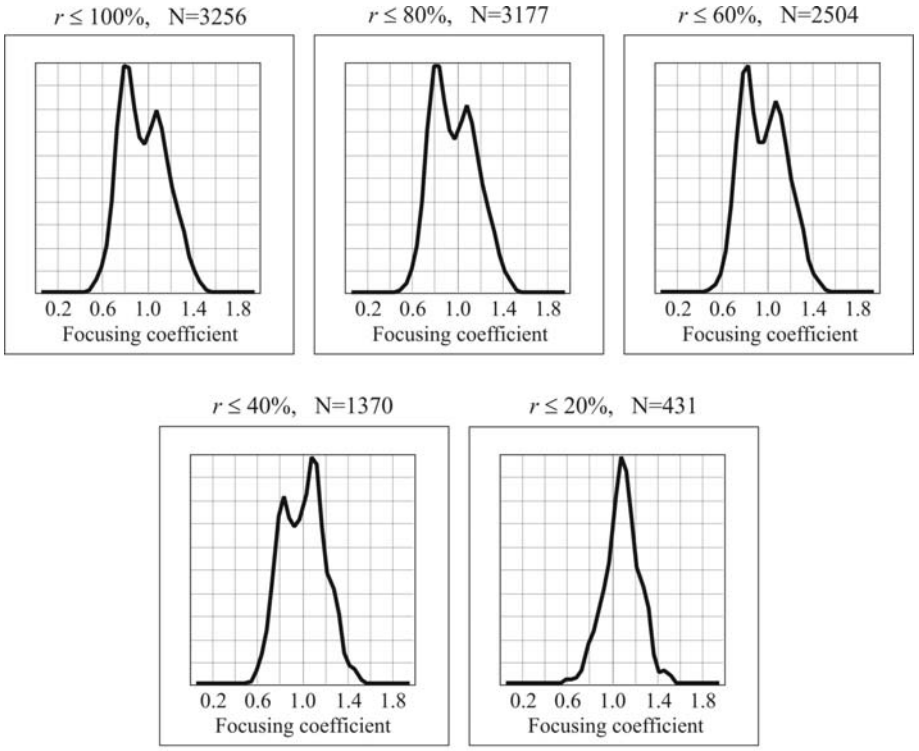

Figure 16. Histograms describing the distribution density of number of measurements with respect to the value of focusing coefficient for different samples according to the error ratio *r*. N is the sample size.

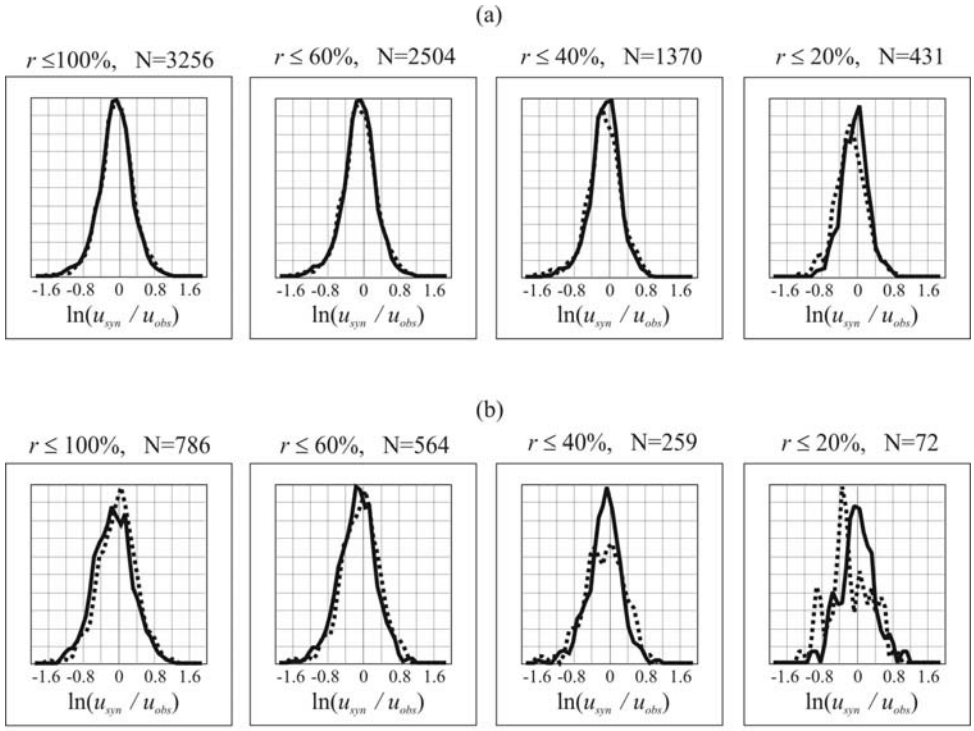

Figure 17. Histograms for $\ln(u_{syn} / u_{obs})$ for mix of four concerned periods (a) for entire range of focusing effect and (b) for strong focusing effect. Solid lines - focusing effect is not taken into account; dashed lines -focusing effect is taken into account. N is the sample size.

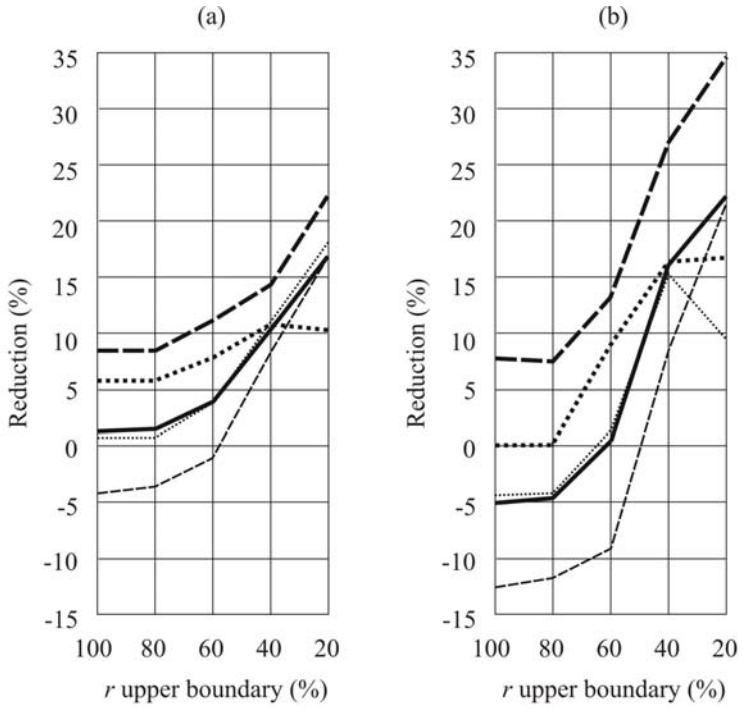

Figure 18. Reduction of relative misfit for different periods: solid lines for mix of four periods, thin dashed lines for 60s, thin dotted lines for 75s, thick dashed lines for 100s, thick dotted lines for 150s. (a) Eentire range of focusing effect, (b) strong focusing effect.

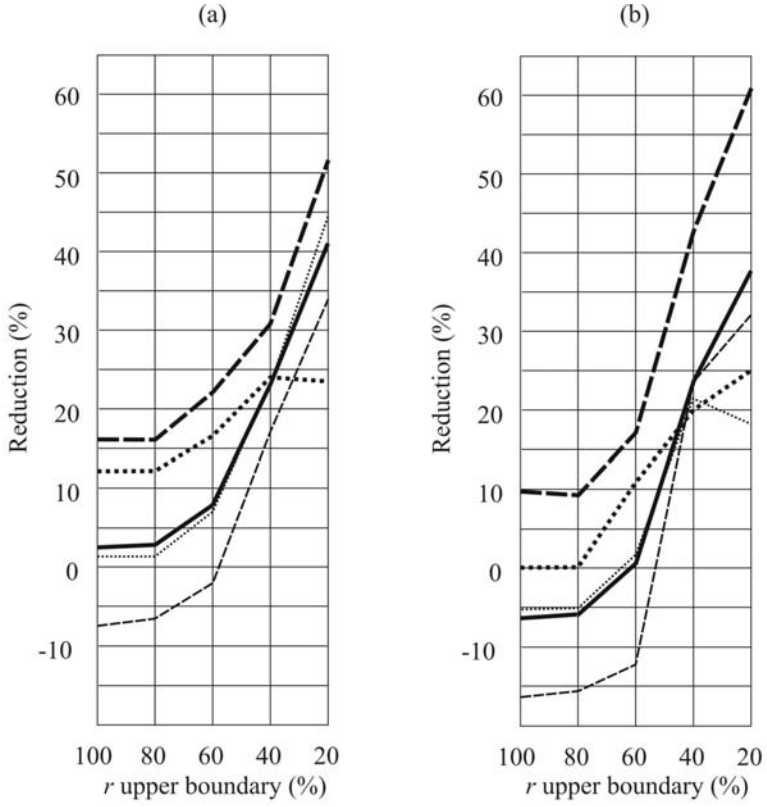

Figure 19. Normalized reduction of relative misfit for different periods. Notations are the same as in figure18. (a)Entire range of focusing effect, (b) strong focusing effect.

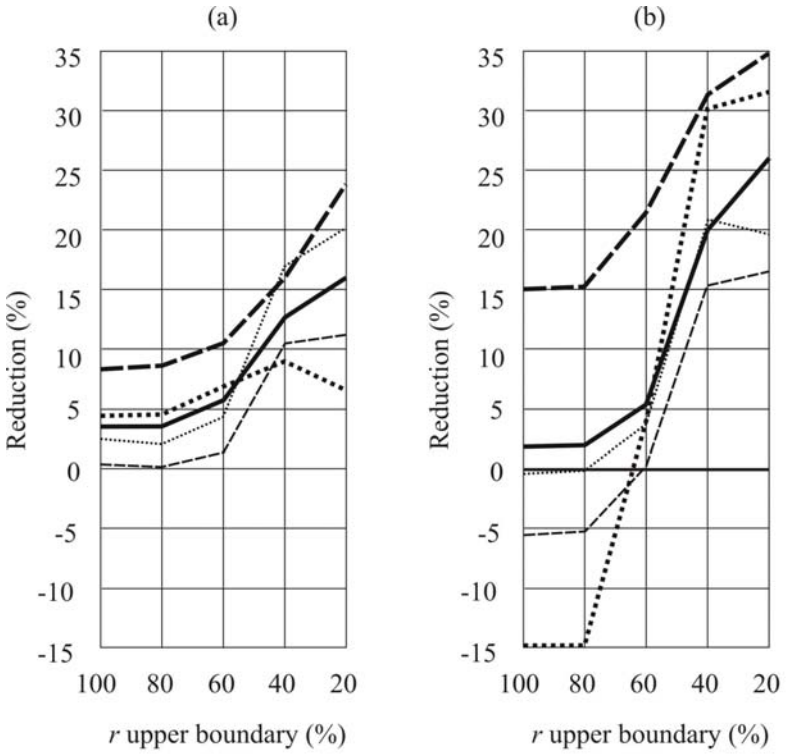

Figure 20. Reduction of absolute misfit (esimate 1) for different periods. Notations are the same as in figure 18. (a) Entire range of focusing effect, (b) strong focusing effect.

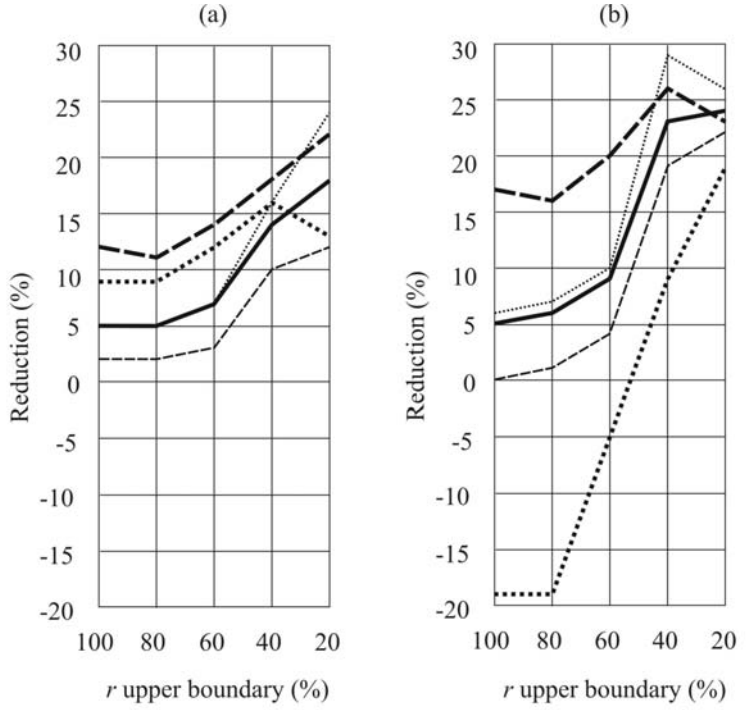

Figure 21. Reduction of absolute misfit (estimate 2) for different periods. Notations are the same as in figure 18. (a) Entire range of focusing effect, (b) strong focusing effect.

References

V.M. Babich, B.A. Chikachev and T.B. Yanovskaya, 1976. Surface waves in a vertically inhomogeneous elastic half-space with weak horizontal inhomogeneity, *Izv. Akad. Nauk SSSR, Fizika Zemli,* 4, 24-31.

G. Backus and M. Mulcahy, 1976. Moment tensors and other phenomenological descriptions of seismic sources. Pt.1. Continuous displacements, *Geophys. J. R. astr. Soc.*, 46, 341-362.

G. Backus, 1977a. Interpreting the seismic glut moments of total degree two or less, *Geophys. J. R. astr. Soc.*, 51, 1-25.

G. Backus, 1977b. Seismic sources with observable glut moments of spatial degree two, *Geophys. J. R. astr. Soc.*, 51, 27-45.

Beucler, E., 2002. Regional and global tomography of the Earth mantle: approach from body and surface waves. *Ph. D. thesis, Institut de Physique du Globe de Paris.*

B.G. Bukchin, 1989. Estimation of earthquake source parameters In: V.I. Keilis-Borok (Editor), Seismic surface waves in a laterally inhomogeneous earth. Kluwer Academic Publishers Dordrecht, 229-245.

B.G. Bukchin, 1990. Determination of source parameters from surface waves recordings allowing for uncertainties in the properties of the medium, *Izv. Akad. Nauk SSSR, Fizika Zemli,* 25, 723-728.

B.G. Bukchin, A.L. Levshin, L.I. Ratnikova, B. Dost and G. Nolet, 1994. Estimation of spatio-temporal source parameters for the 1988 Spitak, Armenia Earthquake, *Computational Seismology and Geodynamics*, 25, English Transl. 156-161, Am. Geophys. Union.

B.G. Bukchin, 1995. Determination of stress glut moments of total degree 2 from teleseismic surface waves amplitude spectra, *Tectonophysics*, 248, 185-191.

Das, S. & Kostrov, B.V., 1997. Determination of the polynomial moments of the seismic moment rate density distributions with positivity constraints, *Geophys. J. Int.*, 131, 115-126.

Gomez, B. Bukchin, R. Madariaga and E.A. Rogozhin, 1997a. A study of the Barisakho, Georgia earthquake of October 23, 1992 from broad band surface and body waves, *Geophyz. J. Int,* V. 129, No. 3, pp 613--623

J.M. Gomez, B. Bukchin, R. Madariaga, E.A. Rogozhin and B.M. Bogachkin, 1997b. Space-Time study of the 19 August 1992 Susamyr earthquake, Kyrgyzstan, Journal of Seismology, V.1, N 3, pp 219-235.

A.V. Lander, 1989. Frequency-time analysis. In: V.I. Keilis-Borok (Editor), Seismic surface waves in a laterally inhomogeneous earth. Kluwer Academic Publishers Dordrecht, 153-163.

Lasserre, C., Bukchin, B., Bernard, P., Tapponnier, P., Gaudemer, Y., Mostinsky, A., and Dailu, R., Sources parameters and tectonic origin of the 1996 June 1 Tianzhu (Mw = 5:2) and 1995 July 21 Yongden (Mw = 5:6) earthquakes near the Haiyuan fault (Gansu, China), Geophys. J. Int., 144 (1), pp 206-220, 2001.

A.L. Levshin, 1985. Effects of lateral inhomogeneity on surface wave amplitude measurements, *Annles Geophysicae*, 3, 4, 511-518.

McGuire, J. J., Zhao, L., and Jordan, T. H., Teleseismic inversion for the second-degree moments of earthquake space-time distributions, Geophys. J. Int., 145 (3), 661-678, 2001.

Ricard Y., H-C. Nataf & J-P. Montagner, 1996. The three-dimensional seismological model a priori constrained: Confrontation with seismic data. *J. Geophys. Res*., 101, pp 8457-6472.

Romanowicz, B., 1995. A global tomographic model of shear attenuation in the upper mantle. *J. Geophys. Res.* Vol. 100, No. B7, pp 12,375-12,394.
Pavlov, V.M., 1994. On non-uniqueness of the inverse problem for a seismic source – II. Treatment in term of polynomial moments, *Geophys. J. Int.*, 119, 497-496.
J.H. Woodhouse, 1974. Surface waves in the laterally varying structure. *Geophys. J. R. astr. Soc.*, 90, 12, 713-728.